The Astrophysical Journal, 615:495–505, 2004 November 1

THE SLOWLY EXPANDING ENVELOPE OF CRL 618 PROBED WITH HC_3N ROTATIONAL LADDERS

J. R. Pardo,[1] J. Cernicharo,[1] and J. R. Goicoechea
Departamento de Astrofísica Molecular e Infrarroja, Instituto de Estructura de la Materia, CSIC, Serrano 121, E-28006 Madrid, Spain

and

T. G. Phillips
Division of Physics, Mathematics, and Astronomy, California Institute of Technology, MS 320-47, Pasadena, CA 91125
Received 2004 May 17; accepted 2004 July 7

ABSTRACT

Lines from HC_3N and isotopic substituted species in ground and vibrationally excited states produce crowded millimeter and submillimeter wave spectra in the C-rich protoplanetary nebula CRL 618. The complete sequence of HC_3N rotational lines from $J = 9–8$ to $J = 30–29$ has been observed with the IRAM 30 m telescope toward this object. Lines from a total of 15 different vibrational states (including the fundamental), with energies up to 1100 cm^{-1}, have been detected for the main HC_3N isotopomer. In addition, the Caltech Submillimeter Observatory telescope has been used to complement this study in the range $J = 31–30$ to $J = 39–38$, with detections in five of these states, all of them below 700 cm^{-1}. Only the rotational lines of HC_3N in its ground vibrational state display evidence of the well-known CRL 618 high-velocity outflow. Vibrationally excited HC_3N rotational lines exhibit P Cygni profiles at 3 mm, evolving to pure emission line shapes at shorter wavelengths. This evolution of the line profile shows little dependence on the vibrational state from which the rotational lines arise. The absorption features are formed against the continuum emission, which has been successfully characterized in this work as a result of the large frequency coverage. The fluxes range from 1.75 to 3.4 Jy in the frequency range 90–240 GHz. These values translate to an effective continuum source with a size between 0.″22 and 0.″27, an effective temperature at 200 GHz ranging from 3900 to 6400 K, and a spectral index between −1.15 and −1.12. We have made an effort to simultaneously fit a representative set of observed HC_3N lines through a model with an expanding shell around the central star and its associated H II region, assuming that LTE prevails for HC_3N. The simulations show that the slowly expanding inner envelope has expansion and turbulence velocities of ∼5–18 and ∼3.5 km s^{-1}, respectively, and that it is possibly elongated. Its inclination with respect to the line of sight has also been explored. The HC_3N column density in front of the continuum source has been determined by comparing the output of an array of models with the data. The best fits are obtained for column densities in the range $(2.0–3.5) \times 10^{17}$ cm^{-2}, consistent with previous estimates from *Infrared Space Observatory* (*ISO*) data, and T_K in the range 250–275 K, in very good agreement with estimates made from the same *ISO* data.

Subject headings: circumstellar matter — ISM: molecules — radio lines: stars — stars: AGB and post-AGB — stars: carbon — stars: individual (CRL 618)

1. INTRODUCTION

CRL 618 is probably the best example of a C-rich protoplanetary nebula with a thick molecular envelope (Bujarrabal et al. 1988) surrounding a B0 star and an ultracompact H II region from which UV radiation impinges on the envelope. Its distance of 1.7 kpc makes this object one of the best-suited sources for studying the evolutionary stages from the asymptotic giant branch (AGB) to planetary nebula (Herpin et al. 2002). The brightening of the H II region in the 1970s (Kwok & Feldman 1981; Martín-Pintado et al. 1993) and the discovery of high-velocity molecular winds (HVMWs) with velocities of up to 200 km s^{-1} (Cernicharo et al. 1989) illustrate the rapid evolution of the central star and its influence on the circumstellar ejected material. From observations of molecular gas at arcsecond resolution, the HVMW and the slowly expanding envelope have been resolved and precisely located around the ultracompact H II region (Neri et al. 1992; Cox et al. 2003; Sánchez-Contreras & Sahai 2004).

The recent discovery of the polyynes HC_4H and HC_6H and of benzene (C_6H_6), the first aromatic molecule detected outside the solar system, in CRL 618 (Cernicharo et al. 2001a, 2001b) emphasize the fact that copious mass ejection toward the end of the AGB phase and the related shock and UV-driven chemistry make C-rich nebulae of this type very efficient factories of organic molecules (see detailed chemical models for this object in Cernicharo [2004]). Small hydrocarbons and pure carbon chains are formed, and they in turn can be the small nuclei from which larger C-rich molecules, such as polycyclic aromatic hydrocarbons, can be built. These molecules are proposed as being responsible for the observed emission labeled as unidentified infrared bands.

In order to draw the clearest picture of the chemical composition, structure, and dynamics of CRL 618, it is necessary to perform complete line surveys in those regions of the electromagnetic spectrum where most molecules emit. One of these line surveys has been carried out by us at millimeter wavelengths with the IRAM 30 m telescope (J. Cernicharo et al. 2004, in preparation). One of the most important features seen in this survey is the presence of clusters of lines with a frequency separation of ≃9 GHz, corresponding to rotational transitions in the ground and vibrationally excited states of HC_3N. This molecule belongs to the cyanopolyynes, $HC_{2n+1}N$, an important group of interstellar molecules (detected in space up to $2n + 1 = 11$; Bell et al. 1997). Because of the relatively

[1] Visiting scientist at Division of Physics, Mathematics, and Astronomy, California Institute of Technology, MS 320-47, Pasadena, CA 91125.

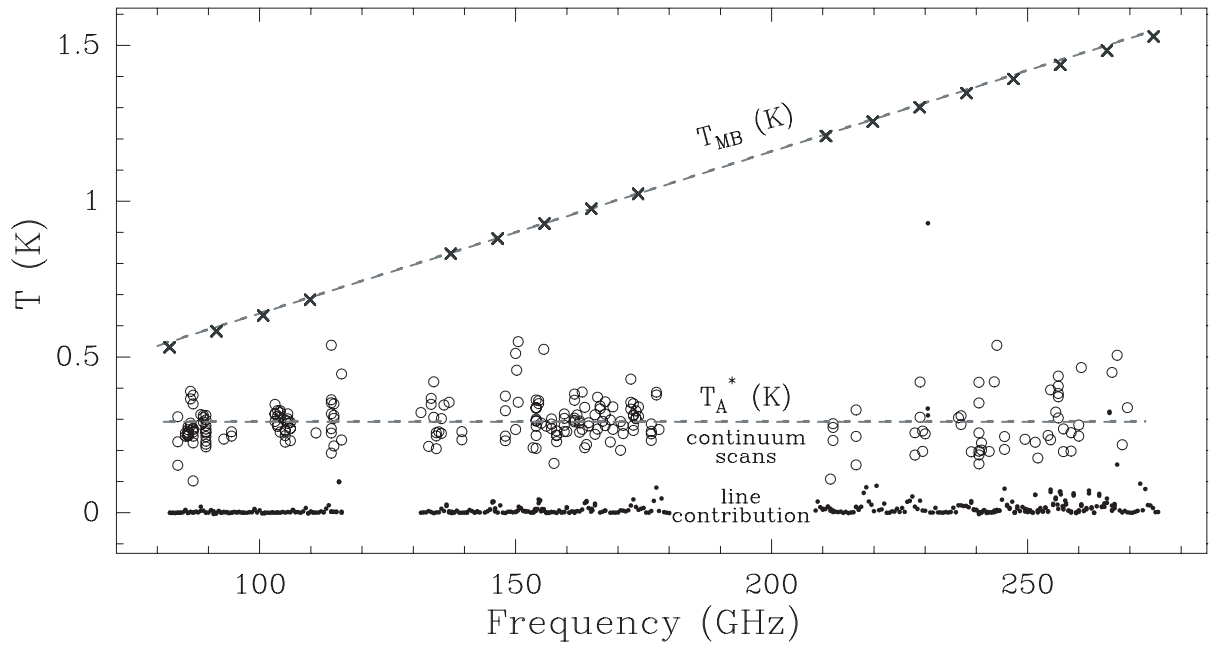

FIG. 1.—Millimeter-wave continuum of CRL 618 observed by the IRAM 30 m telescope (*circles*; T_A^* scale, from pointing observations on CRL 618 in continuum mode). Also shown are the fit of these data to a horizontal line (*horizontal dashed line*) and translated into T_{MB} (*inclined dashed line*) and the continuum T_{MB} simulated by our model (*crosses*; see §§ 5.1 and 5.2).

low energy of their bending modes, they can be found in space in many vibrationally excited states. As an example, Wyrowski et al. (1999) detected HC_3N in 11 vibrationally excited states with energies up to 1100 cm^{-1} toward the ultracompact H II region G10.47+0.03. The small frequency spacings of the HC_3N rotational transitions make this molecule an interesting tool for probing the physical conditions of molecular gas in C-rich circumstellar shells such as in CRL 618. The HC_3N line profiles in this object show the interesting behavior of evolving with frequency from P Cygni to normal emission. This is presented and analyzed in this paper using a model, under LTE, for an expanding envelope of azimuthally symmetric geometry around a continuum source.

In § 2 we present the IRAM 30 m and Caltech Submillimeter Observatory (CSO) observation procedures. The spectroscopy of HC_3N is briefly summarized in § 3. The results of the observations, including discussions about the continuum emission and the velocity components of the HC_3N lines, are found in § 4. In § 5 we present the model that has been built to explore the physical conditions. Simulations are presented and discussed. Finally, the conclusions are presented in § 6.

2. OBSERVATIONS

The CRL 618 observations presented in this paper are part of a line survey carried out with the IRAM 30 m telescope and complemented by the CSO (J. Cernicharo et al. 2004, in preparation).

The IRAM 30 m telescope currently has the largest effective aperture operating at the 3, 2, and 1.3 mm atmospheric windows. The observations started in 1994 and were completed in the winter of 2001–2002. In order to avoid confusion between the signal and the image sidebands, the receivers were optimized for rejection of image sidebands larger than 12 dB, which resulted in practically no sideband contamination, except for just a few cases in which a very intense line (CO, HCN, . . .) was present in the image sideband. Receivers covered the following frequency ranges (in GHz): 82–116, 130–184, 201–258, and 240–279. The pointing and focus were always checked on the target source, since CRL 618 exhibits a continuum of about 0.3 K in the T_A^* scale of the IRAM 30 m telescope across the surveyed frequency range (see Fig. 1). The pointing was kept within 2″ accuracy. We carried out the observations using the wobbler-switching mode with offsets of 60″ and frequencies of 1 Hz in order to obtain very flat baselines. This is very important because some spectra are so crowded with lines that their reduction could be difficult otherwise (not enough baseline). The back ends used were two 512 MHz filter banks connected to the receivers, operating below 200 GHz, and a 512 MHz autocorrelator with a channel width of 1.25 MHz connected to the others. System temperatures were typically 100–400 K at 3 mm, 200–600 K at 2 mm, and 300–800 K at 1.3 mm.

The observations performed in several observing runs in 2000, 2001, and 2002 with the 10.4 m dish of the CSO at the summit of Mauna Kea (Hawaii) made use of a helium-cooled SIS receiver operating in double-sideband mode in the frequency range 280–360 GHz. The continuum emission from CRL 618 at the CSO has a level of 0.05–0.06 K in the T_A^* scale, too low to allow pointing on the source. The pointing was therefore checked on the available planets and was kept within 3″–4″ accuracy (the half-power beamwidth ranged from 20″ to 25″). The system temperatures varied from 500 to 1200 K. In order to obtain flat baselines we used the secondary mirror chopping technique at a frequency of about 1 Hz and an offset of 90″. In order to discriminate whether the lines were from the signal or from the image sideband, the observations were made twice with a frequency shift of a few tens of MHz (usually 50).

3. HC_3N SPECTROSCOPY

The rotational spectrum of cyanoacetylene, HC_3N, has been investigated in vibrational states up to about 1750 cm^{-1} by Mbosei et al. (2000). The resulting database for this molecule has been provided to us by A. Fayt. This work has been recently published (Fayt et al. 2004). The frequencies have been checked against our millimeter wave line survey and show a remarkable agreement in the detected vibrational states.

There are three doubly degenerate bending modes of HC_3N, ν_5, ν_6, and ν_7 in order of decreasing energy (223, 499, and 663 cm^{-1}). When considering the rotation, their degeneracy is broken as a result of the direction of the rotation axis. This is known as *l*-doubling. The mode ν_4 is the lowest energy stretching mode (880.6 cm^{-1}). The other three vibrational (stretching) modes have energies above 2000 cm^{-1} and are not seen in CRL 618. In this work, we have been able to detect HC_3N pure rotational lines in the ground state and in 14 different vibrationally excited states. Detections have also been obtained in a number of isotopomers, but they will be discussed in a separate work.

The lines are labeled by the rotational quantum numbers (J_{up}–J_{low}), the vibrational quantum numbers ($v_4v_5v_6v_7$), and the *l*-doubling parameters [l_5 l_6 l_7]. Table 1 provides the observed line parameters (velocity, width, and integrated area) of a pair of rotational transitions ($J = 12$–11 and $J = 26$–25) for all detected vibrationally excited states. The $J = 12$–11 lines always display an absorption feature centered at approximately -27.5 km s^{-1} accompanied by weaker emission (undetected in some cases) centered around the LSR velocity of the source. In the $J = 26$–25 lines the absorption is barely detected, and the emission is always much stronger. The selected rotational numbers are representative of the two different types of line profiles observed in HC_3N and in other molecules toward CRL 618.

4. RESULTS

Of the complete frequency survey, as described in § 2, the data set used for the analysis presented in this paper consists of the following:

1. The continuum measured in each setting across the frequency ranges covered: 80–116.5, 132–177, and 204–276 GHz.
2. Those spectra containing HC_3N rotational lines in a subset of vibrational states, selected to sample the range of the vibrational energies among those detected. The selected vibrational states are (0000), (0001), (0002), (0010), (0100), (0003), (0011), (1000), (0012), and (0102) with vibrational energies of 0, 223, 446, 499, 663, 669, 722, 881, 945, and 1109 cm^{-1}, respectively.

4.1. *Continuum Emission*

The central star has an effective temperature of 30,000 K, and it is surrounded by an H II region and its photodissociation region. Continuum emission from the H II region and the dust affect the population of the molecular levels and has to be taken into account in modeling the source. The properties of the measured continuum are discussed in this section.

The level of continuum emission is important to explaining the features seen in the line profiles of many molecules in CRL 618. Although the wobbler-switching method used with the 30 m telescopes for this work should provide in principle a precise continuum level for each spectrum directly, the continuum levels of different spectra never match perfectly. Moreover, earlier work has shown evidence of variability over several years (see below). Therefore, we have decided to use all the pointing data to retrieve the continuum by fitting Gaussians to the pointing scans and storing the peak of the fitted Gaussian (in T_A^* scale) and the central frequency. The obvious bad scans and those for which the pointing errors were larger than 2″ have been ignored. The results are shown in Figure 1 (*circles*). The quantity T_{MB} and the fluxes have been derived from a linear fit to those data (actually, a horizontal line), scaled by the corresponding beam and forward efficiencies of the 30 m telescope. In principle, this analysis could be affected by the presence of lines. However, the total flux from the lines represents less than 3%–5% of the continuum in most frequency settings. We have just ignored the few frequency settings with very strong lines, such as the lowest rotational transitions of CO and HCN. In total flux our measurements give 1.75 Jy at 90 GHz, 2.4 Jy at 150 GHz, and 3.4 Jy at 240 GHz.

Several continuum measurements of CRL 618 at different frequencies exist. In an early interferometric mapping carried out at centimeter wavelengths with the Very Large Array (VLA), it was shown that the compact radio source had a size of $0\farcs4 \times 0\farcs1$ (Kwok & Bignell 1984). Using the VLA at 23 GHz, Martín-Pintado et al. (1993, 1995) found an elliptical source with a size of $0\farcs40 \times 0\farcs12$ and an integrated flux density of 189 ± 20 mJy (peak continuum flux of 16.7 mJy $beam^{-1}$) in 1993 and 250 ± 20 mJy in 1995. Thorwirth et al. (2003) found 26.3 ± 3 mJy at 4488.48 MHz and 750 ± 75 mJy at 40 GHz with a size of $0\farcs34 \times 0\farcs16$ (peak continuum flux of 140 mJy $beam^{-1}$). At 1.3 mm, Walmsley et al. (1991) found fluxes varying from 1.0 to 3.3 Jy between 1987 and 1990. If this variability is real, it could explain part of the scattering in the data points presented in Figure 1 (obtained over several winters). Earlier work (Kwok & Feldman 1981; Spergel et al. 1983) also presents the source as variable at centimeter wavelengths. Other measured fluxes found in the literature include Shibata et al. (1993), who measured 1.48 Jy at 115 GHz, and Martín-Pintado et al. (1988), who at 22.3, 87.6, 147.0, and 231.9 GHz measured 0.24 ± 0.02, 1.1 ± 0.1, 1.8 ± 0.2, and 2.0 ± 0.3 Jy, respectively, values about 25%–32% smaller than our own results (see Fig. 1), which represent an average over at least 4 years.

From the line survey currently underway in the 280–360 GHz range, the measured continuum emission averages to 0.06–0.07 K in the T_A^* scale ($\sim$0.1 K in T_{MB}). This result agrees with the trend observed at the higher end of the IRAM 30 m survey (275 GHz) given the smaller size of the CSO antenna (10.4 m).

4.2. HC_3N *Ground Vibrational State*

The profiles of HC_3N rotational lines within the ground vibrational state (see Fig. 2) show evidence of the HVMW, also seen in lines of CO and other molecules. In HC_3N, the HVMW component of the line profile extends some 200 km s^{-1} in some cases (see Fig. 3). In addition to this one, there is another component associated with a slowly expanding molecular envelope around the ultracompact H II region. This component has an FWHM of about 18 km s^{-1} and is approximately centered at the LSR velocity of CRL 618 (-21.3 km s^{-1}). Two different absorption dips are present (see Fig. 2). The first one appears at -37 km s^{-1} in all lines up to at least $J = 37$–36. It turns out that this feature is related to the [1 0 0]E component of the rotational transitions of the (0100) state. The other absorption feature at -55 km s^{-1} is due to expanding gas in the line of sight of the continuum source and is also found in low-*J* HCN (Neri et al. 1992) and CO (Cernicharo et al. 1989; Herpin et al. 2002). On the red side of the line, between approximately -8 and -7 km s^{-1}, there is evidence of emission that Neri et al. (1992) attributed to an unresolved structure located to the northeast of the H II region.

4.3. *Vibrationally Excited* HC_3N

4.3.1. *The (0001) Vibrational State*

The HC_3N rotational lines in the (0001) vibrational level, at least below $J_{up} \sim 20$, still trace gas at higher velocities than

TABLE 1

OBSERVED LINE PARAMETERS OF THE $J = 12-11$ AND $J = 26-25$ TRANSITIONS IN ALL VIBRATIONALLY EXCITED STATES OF HC_3N DETECTED TOWARD CRL 618

			$J = 12$–11							$J = 26$–25						
STATE (1)	E (2)	TRANSITION (3)	ν (4)	v_1 (5)	Δv_1 (6)	A_1 (7)	v_2 (8)	Δv_2 (9)	A_2 (10)	ν (11)	v_1 (12)	Δv_1 (13)	A_1 (14)	v_2 (15)	Δv_2 (16)	A_2 (17)
(0001).....	223	[0 0 1]F	109.598825	−20.9	14.9	3.6	−31.6	22.3	−3.3	237.432241	−20.8	18.7	7.2			
	223	[0 0 1]E	109.442011[a]							237.093375						
(0002).....	426	[0 0 0]E	109.865960[b]							237.968847	−23.7	16.0	5.9			
	426	[0 0 2]E	109.870288[c]							238.053887	−21.6	11.3	3.5			
	426	[0 0 2]F	109.865960[d]							238.010133	−21.5	10.6	3.2			
(0010).....	499	[0 1 0]E	109.352748	−21.3	7.4	0.47	−29.8	7.3	−0.90	236.900342						
	499	[0 1 0]F	109.438718[e]							237.086494						
(0100).....	663	[1 0 0]E	109.183008[f]							236.529566[f]						
	663	[1 0 0]F	109.244206	−21.3	11.0	0.35	−28.4	6.6	−0.66	236.661402	−20.5	8.4	0.44			
(0003).....	669	[0 0 1]E	110.050809	−21.3	9.0	0.37	−28.7	6.9	−0.59	238.401147	−21.2	7.47	1.0			
	669	[0 0 3]E+F	110.211793	−21.3	4.1	0.02	−29.5	7.7	−0.79	238.771331	−21.3	12.0	1.8	−31.1	5.8	−0.3
	669	[0 0 1]F	110.366468	−21.3	14.6	0.7	−28.3	6.2	−0.62	239.082313	−20.9	11.5	1.4			
(0011).....	721	[0 1 −1]E	109.736687[g]							237.681318	−22.1	9.2	1.5	−28.2	14.2	−0.7
	721	[0 1 −1]F	109.740137[h]							237.713612[i]						
	721	[0 1 1]F	109.749784[j]							237.783921	−21.8	9.9	1.9	−26.9	15.5	−1.0
	721	[0 1 1]E	109.752621[k]							237.814870	−22.9	8.6	1.4	−28.3	11.0	−0.7
(1000).....	880	[0 0 0]E	109.023292	−21.3	12.7	0.22	−27.9	6.2	−0.40	236.184052	−23.6	8.8	0.35	−27.8	4.1	−0.22
(0101).....	886	[1 0 −1]F	109.558099	−21.3	6.0	0.07	−28.0	4.5	−0.25	237.336037	−21.3	12.0	0.73	−29.0	5.2	−0.30
	886	[1 0 −1]E	109.549318	−21.3	7.5	0.16	−27.5	3.9	−0.18	237.409821[l]						
	886	[1 0 1]F	109.564687	−21.3	7.5	0.16	−27.5	5.5	−0.29	237.716883[m]						
	886	[1 0 1]E	109.553091				−27.5	3.9	−0.18	237.898318	−19.8	11.4	1.04			
(0004).....	892	[0 0 0]E	110.543693	−21.3	10.9	0.2	−27.4	5.2	−0.35	239.370230	−21.1	8.8	0.63			
	892	[0 0 2]F	110.548972							239.125296						
	892	[0 0 4]E+F	110.554367	−21.3	7.1	8.9	−28.6	4.8	−0.23	239.510881						
	892	[0 0 2]E	110.562578	−19.9	10.5	0.6				238.962431						
(0012).....	944	[0 1 0]E	109.989997				−27.4	5.2	−0.30	238.254341	−21.7	8.1	0.53			
	944	[0 −1 2]F	110.035645				−28.2	4.5	−0.18	238.388217	−20.2	9.3	0.64			
	944	[0 1 2]E+F	110.097528	−21.3	5.7	0.09	−27.8	5.6	−0.34	238.526950	−22.5	8.5	0.58	−31.2	6.1	−0.28
	944	[0 −1 2]E	110.148765	−21.3	5.0	0.06	−27.7	4.7	−0.16	238.631641	−21.5	8.8	0.79			
	944	[0 1 0]F	110.189752				−27.2	5.0	−0.18		−21.2	9.5	0.75			

TABLE 1—*Continued*

			J = 12–11							J = 26–25						
State (1)	E (2)	Transition (3)	ν (4)	v_1 (5)	Δv_1 (6)	A_1 (7)	v_2 (8)	Δv_2 (9)	A_2 (10)	ν (11)	v_1 (12)	Δv_1 (13)	A_1 (14)	v_2 (15)	Δv_2 (16)	A_2 (17)
(0020).....	998	[0 0 0]E	109.522442				−27.4	4.3	−0.17	237.270155						
	998	[0 2 0]E	109.616120	−21.3	7.5	0.23	−29.4	7.7	−0.38	237.468947	−21.3	8.2	0.77			
	998	[0 2 0]F	109.616295	−21.3	7.2	0.24	−28.8	8.3	−0.41	237.470747	−19.1	7.5	0.73			
(1001).....	1103	[0 0 1]E	109.306687				−27.0	6.0	−0.17	236.795297	−20.0	4.5	0.10	−28.5	4.4	−0.12
	1103	[0 0 1]F	109.469407				−27.0	6.0	−0.12	237.145656	−21.3	9.5	0.27			
(0102).....	1109	[−1 0 2]E	109.789853[n]							237.803492	−19.9	5.3	0.25			
	1109	[1 0 0]F	109.847627[n]							237.956672[o]						
	1109	[1 0 2]E	109.905021[n]							238.164654	−20.3	5.6	0.22			
	1109	[1 0 2]F	109.868821[n]							237.995859[p]						
	1109	[1 0 0]E	109.953634[n]							238.178301	−21.8	8.6	0.39			
	1109	[−1 0 2]F	109.989048[n]							238.318310						
(0005).....	1115	[0 0 1]E	110.655045	−21.3	11.7	0.1	−28.2	4.8	−0.13	230.471871	−21.3	7.9	0.23	−28.5	4.6	−0.14
	1115	[0 0 1]F	111.131162	−21.3	15.6	0.26	−27.5	2.8	−0.07	231.456018						
	1115	[0 0 5]E+F	110.895474				−28.2	4.8	−0.13	231.009985						
	1115	[0 0 3]E+F	110.902009	−21.3	2.7	0.02	−28.2	5.0	−0.13	231.031080						

Notes.—See the text for notation. In addition to the vibrational states shown here, the (0111) state is tentatively detected at more than 1200 cm^{-1}. Col. (1): Vibrational state. Col. (2): Energy in cm^{-1}. Col. (3): Type of *l*-transition. Cols. (4), (11): Line frequency in GHz. Cols. (5), (12): Position for the emission in km s^{-1}. Cols. (6), (13): Width for the emission in km s^{-1}. Cols. (7), (14): Area for the emission in K km^{-1}. Cols. (8), (15): Position for the absorption in km s^{-1}. Cols. (9), (16): Width for the absorption in km s^{-1}. Cols. (10), (17): Area for the absorption in K km^{-1}.

[a] Blended with (0010)[0 1 0]F.
[b] Blended with [0 0 2]E, F.
[c] Blended with [0 0 2]F, [0 0 0]E.
[d] Blended with [0 0 2]E, [0 0 0]F.
[e] Blended with (0010)[0 1 0]F.
[f] Blended with the ground state of HC_3N.
[g] Line ∼3 MHz away from [0 1 −1]F.
[h] Line ∼3 MHz away from [0 1 −1]E.
[i] Blended with (0101)[1 0 1]F.
[j] Line ∼3 MHz away from [0 1 1]E.
[k] Line ∼3 MHz away from [0 1 1]F.
[l] Blended with (0001)[0 0 1]F.
[m] Blended with (0011)[0 1 −1]F.
[n] Blended with $C^{18}O$.
[o] Blended with (0002)[0 0 0]E.
[p] Blended with (0002)[0 0 2]F.

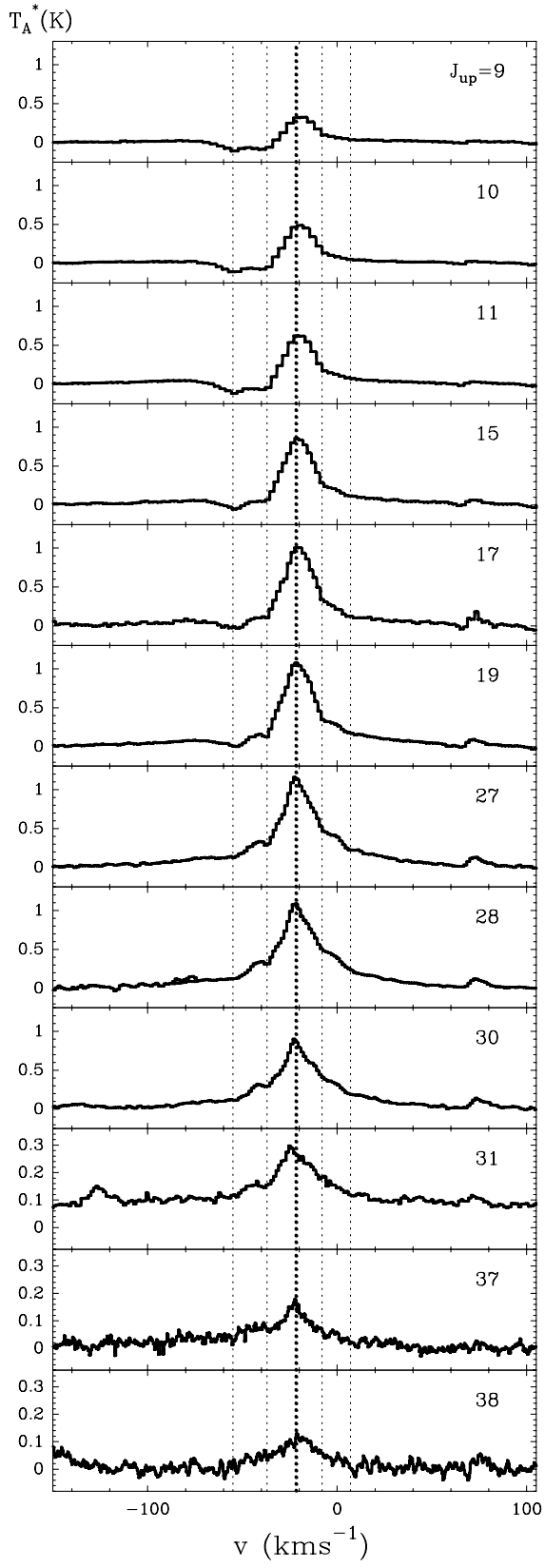

FIG. 2.—HC_3N pure rotational lines toward the protoplanetary nebula CRL 618 in the ground vibrational state. The thick dotted line marks the LSR velocity of the source. The thin dotted lines mark interesting features in the line profile discussed in the text.

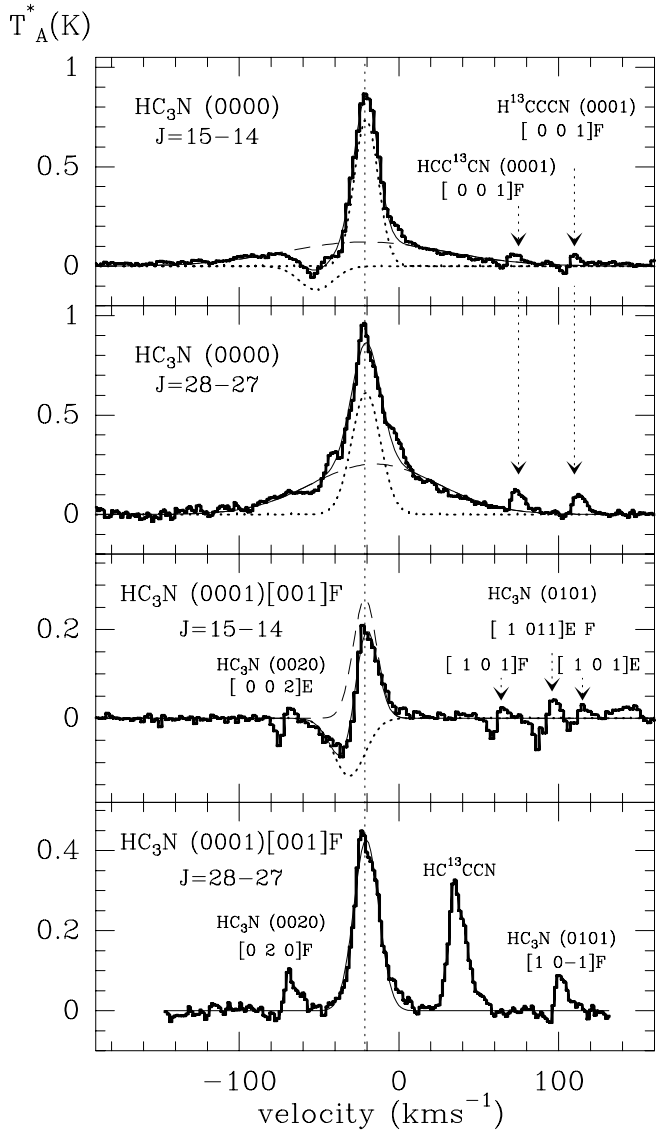

FIG. 3.—Velocity components of HC_3N lines toward CRL 618. In the ground vibrational state (*top two panels*), we see broad wings associated with the HVMW discovered by Cernicharo et al. (1989) and a narrower emission due to the slowly expanding gas envelope around the H II region. A blending with HC_3N (0100) causes the absorption feature at approximately -37 km s^{-1}. The absorption centered at -55 km s^{-1} is also seen in other abundant molecules such as HCN and CO. In vibrationally excited states (*bottom two panels*) the HVMW component is not visible. At low-J the absorption of the slowly expanding gas in front of the continuum source is seen centered at approximately -27 km s^{-1}. However, the absorption disappears at $J > 20$ for the particular case of the (0001) state (the J-number for which this happens depends slightly on the vibrational state). Still, rotational lines within the (0001) state trace velocities larger than those in higher vibrational states, although it is not the HVMW.

that seen in rotational lines corresponding to higher energy vibrational levels (see below). For example, the $J = 15{-}14$ transition in (0001) shows an absorption dip that clearly starts below -50 km s^{-1}, more than 30 km s^{-1} apart from the LSR velocity of the source (see Fig. 3). However, for J_{up} above 20, this colder and faster outflow is not significant in the level population anymore.

4.3.2. *Other Vibrational States*

The HC_3N lines in the rest of the detected vibrationally excited states display patterns with many common characteristics.

The lines appear dominantly in emission at 1.3 mm (at the IRAM 30 m radio telescope) and at shorter wavelengths (CSO observations at 0.850 mm) with an FWHM ranging from 5 to 16 km s^{-1} but mostly around 8–10 km s^{-1}. However, the majority of lines in the 2 and 3 mm windows show P Cygni profiles, with the absorption part being systematically deeper at lower frequencies. This absorption is centered in the range of -26 to -31 km s^{-1}, as expected for an expanding envelope with velocities around 5–10 km s^{-1} surrounding the central continuum source at the LSR velocity of CRL 618. The absorption becomes less deep and shifts to more negative velocities as the emission part gets stronger with increasing J. At frequencies well below 80 GHz, almost all lines, from other species as well, appear strictly in absorption. The velocity of the absorption feature in HC_3N rotational lines with $J_{up} < 7$, in different vibrationally excited states, observed with the Effelsberg 100 m radio telescope (Wyrowski et al. 2003) is around -26 or -27 km s^{-1}. Thorwirth et al. (2003) also report HCN $\Delta J = 0$, l-doubling transitions purely in absorption at the same velocity, as do Martín-Pintado et al. (1995) for NH_3 (3, 3). The lowest transitions we have observed ($J = 9$–8, $J = 10$–9) in some highly excited vibrational states such as (0100) and (1000) do not show emission, and the absorption feature is also centered around -27.5 km s^{-1}.

5. DISCUSSION

In this work we assume that the bulk of vibrationally excited HC_3N emission comes from a compact envelope expanding at about 10 km s^{-1} around the central continuum source. The availability of rotational ladders in so many different vibrationally excited HC_3N states should provide quite a precise picture of the size ratio of the slowly expanding gas region with respect to the continuum source, the shape of the envelope, the temperature profile, the velocity field, and the HC_3N density distribution. All this is explored in §§ 5.1 and 5.2.

5.1. *Model*

In order to reproduce the observed rotational HC_3N ladders, we have built a model, for LTE conditions, of an expanding envelope around a continuum source. Because of blending with the selected HC_3N lines for the analysis, we have also introduced HC_5N, with an abundance ratio one-third that of HC_3N (Cernicharo et al. 1987; Guélin & Cernicharo 1991), and isotopic species of HC_3N using a $^{12}C/^{13}C$ ratio of 15.

The lines are formed as follows: First, the central continuum source is responsible for the observed continuum level. The gas situated between the continuum source and the Earth absorbs that continuum and also emits. The gas in regions outside the line of sight to the continuum source contributes by emission only. The continuum source is considered opaque to the emission of the gas behind it. The spectrum of the continuum source and its size ratio with respect to the gas region turn out to be key parameters to fitting the simulations to the observed HC_3N rotational lines. The absorption takes place primarily at the terminal velocity of the expanding envelope in front of the continuum source. The emission can help to "fill" the absorption dip depending on the characteristics of the velocity field and the turbulence velocity.

The simplest model considers a spherical expanding envelope of gas surrounding a central continuum source (also spherical). The envelope is divided into different shells, where the total HC_3N number density and the temperature vary according to a power law, and radial expansion and turbulent

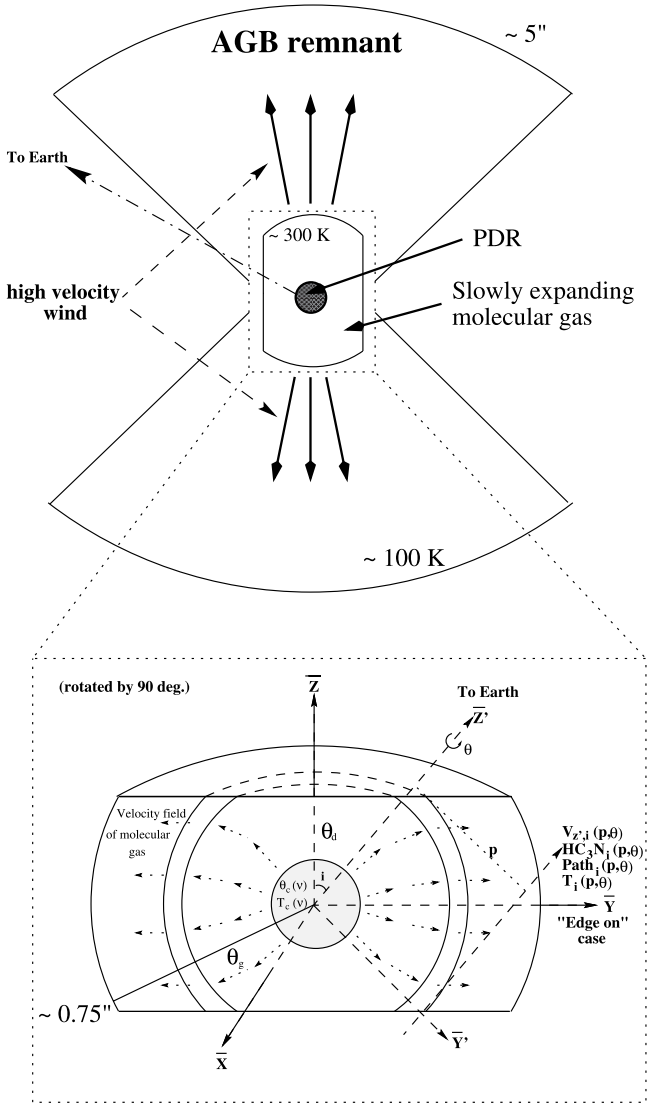

FIG. 4.—Model of CRL 618 including the description of the expanding elongated structure considered to account for the observed HC_3N line profiles. See the text for details about the different parameters of the model.

velocities are linearly interpolated between input values at the boundaries. Such a simple model can only approximately reproduce the main observational characteristics of the HC_3N rotational ladders in CRL 618. A more complex model has been developed to account for an elongated envelope with nonradial velocity components. We consider an external angular size of the (spherical) slowly expanding envelope θ_g, and then we truncate it so that, in the truncation direction, the size is $\theta_d = \theta_g r_d$, where r_d is the truncation parameter (see Fig. 4). Other geometric details of this model are as follows: A coordinate system (X, Y, Z) is defined with the Z-axis running in the direction in which the sphere is truncated and with X and Y orthogonal to each other and to Z. The velocity field is a function of $[(x^2 + y^2)^{1/2}, z]$ (azimuthal symmetry in the X-Y plane), and the temperature and gas densities are functions only of $r = (x^2 + y^2 + z^2)^{1/2}$ (radial symmetry). The second coordinate system has the axis X' in common with the X-axis just described, and the remaining two coordinates (Y', Z') are rotated with respect to (Y, Z) by an angle i so that Z' points to the Earth (line of sight). The "edge-on" case therefore corresponds to $i = 90°$. The continuum source is spherical, with an angular radius θ_c. The value of θ_c has to be in the range 0.″15–0.″4 in

TABLE 2
SET OF MODELS TO DESCRIBE THE CENTRAL CONTINUUM SOURCE OF CRL 618 ACCORDING TO THE PARAMETERS DEFINED IN EQ. (1)

Size (arcsec)	T_{cont} (200 GHz)	Spectral Index s
0.18.....	8600	−1.15
0.22.....	6400	−1.15
0.27.....	**3900**	**−1.12**
0.32.....	3200	−1.12
0.36.....	2300	−1.12

NOTE.—The preferred model is in bold (see Fig. 1).

order to be compatible with the data presented in § 4.1. We use as an input parameter its ratio r_c with respect to the external angular size of the slowly expanding envelope, $r_c = \theta_c/\theta_g$. The effective temperature of the continuum source would depend on that size in order to match the observed continuum. In general, the equivalent size θ_c would be a function of frequency. However, a constant size and a frequency-dependent T_c, characterized by a spectral index s (see following equation), fit the data very nicely (see Fig. 1 and Table 2):

$$T_{\rm cont}(\nu) = T_{\rm cont}(200\ {\rm GHz})(\nu/200\ {\rm GHz})^s. \qquad (1)$$

In the elongated envelope case, the velocity field cannot be exactly radial: $\boldsymbol{v} = v_r\boldsymbol{r} + v_{xy}\boldsymbol{r}_{xy}$ ($v_{xy} \neq 0$ if $r_d < 1$). The extra velocity component in the X-Y plane makes the velocity pattern look as in Figure 4. This kind of velocity field has the advantage of having gas with the same velocity projection in regions inside and outside the column between the continuum source and the Earth. Some extra gas is thus allowed to contribute to filling the absorption dip (not only the turbulence velocity helps to do this; see Fig. 5). The velocity field remains unchanged by rotation with respect to the Y- or Z-axis. Therefore, in the $i = 0^\circ$ and 90° cases ("edge-on" or "orthogonal" envelope cases), only the radiative transfer results, as a function of the impact parameter p (defined as an angle), have to be used in the numerical convolution with the antenna beam pattern. If i takes any intermediate value, the numerical integration becomes dramatically more time consuming (10–100 times) because the azimuthal symmetry with respect to the X-Y' plane is broken, and the convolution has to be performed in both p and $\theta_{XY'}$ (the azimuthal angle around the Z' or line-of-sight axis; see Fig. 4).

As we have seen, the model has an important number of parameters. Some of them can be fixed with some confidence, based on data such as the continuum flux (see Fig. 1) and the estimated distance to the source. The other parameters, velocity field, kinetic temperature, shape of the slowly expanding envelope, ratio between its size and that of the continuum source, and HC_3N column density, can be constrained by running a number of models. It is quite straightforward to find the best values for all parameters, with the exception of the kinetic temperature and HC_3N column density. This is discussed below.

5.2. *Constraining the Physical Parameters*

The first step in the simulation process concentrates on the continuum source. We have considered different sizes for it (constant with frequency) and have calculated its effective temperature at a reference frequency (200 GHz) and spectral index s to match the observed continuum (Fig. 1). Based on the references given in § 4.1, the range of sizes we have explored is 0.″15–0.″40. The results are given in Table 2. For each set of values, the fit to our continuum data is very good, typically as shown in Figure 1. As the external size of the gas region we are modeling is around 1.″5 and the ratio of this size to the continuum source size is a key parameter for reproducing the observed line profiles, the preferred values among the five given alternatives are highlighted in bold face.

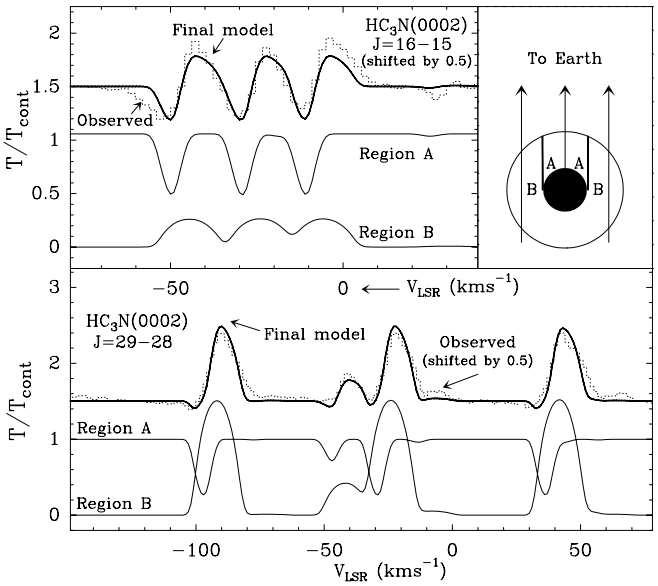

FIG. 5.—Fit of the observed HC_3N rotational line toward CRL 618 and the separate contribution from gas inside and outside the line of sight to the continuum source. The physical parameters correspond to those listed in Table 3.

As the number of physical parameters and lines observed are both large, a general numerical fit to constrain all physical parameters simultaneously is not possible. Rather, it is necessary to run a large number of models in several steps in order to find a reasonable match to all the observed HC_3N rotational ladders. As this is very time consuming, the simulations have been restricted to the (0002), (0010), (0100), (0003), (0011), (1000), (0012), and (0102) vibrational states, as explained in § 4.

In the search for the best solution we also need to define a parameter to evaluate the quality of the fit. Ideally, this parameter has to give equal weight to the different lines, independently of the frequency resolution. We thus define an overall χ as

$$\chi = \frac{1}{N_l}\sum_i \sqrt{\frac{\sum_j |Y_d - Y_m|^2}{N_{\rm ch}}}, \qquad (2)$$

where N_l is the number of suitable lines in Figure 6, $Y_d(j)$ are the data (total flux divided by the continuum flux), $Y_m(j)$ are the model results, and $N_{\rm ch}$ is the number of channels, where $Y_m(j) \neq 1.0$ (i.e., we do not consider channels in which the signal is just the continuum level or lines from species other than HC_3N or HC_5N). In addition, if a line from another chemical species overlaps with those from HC_3N or HC_5N, the corresponding spectrum is discarded. Note also that in Figure 6 not all the l-type lines are shown in each case because of the sometimes large velocity separation. Only the data shown in the figure are used to calculate χ. Blending between different

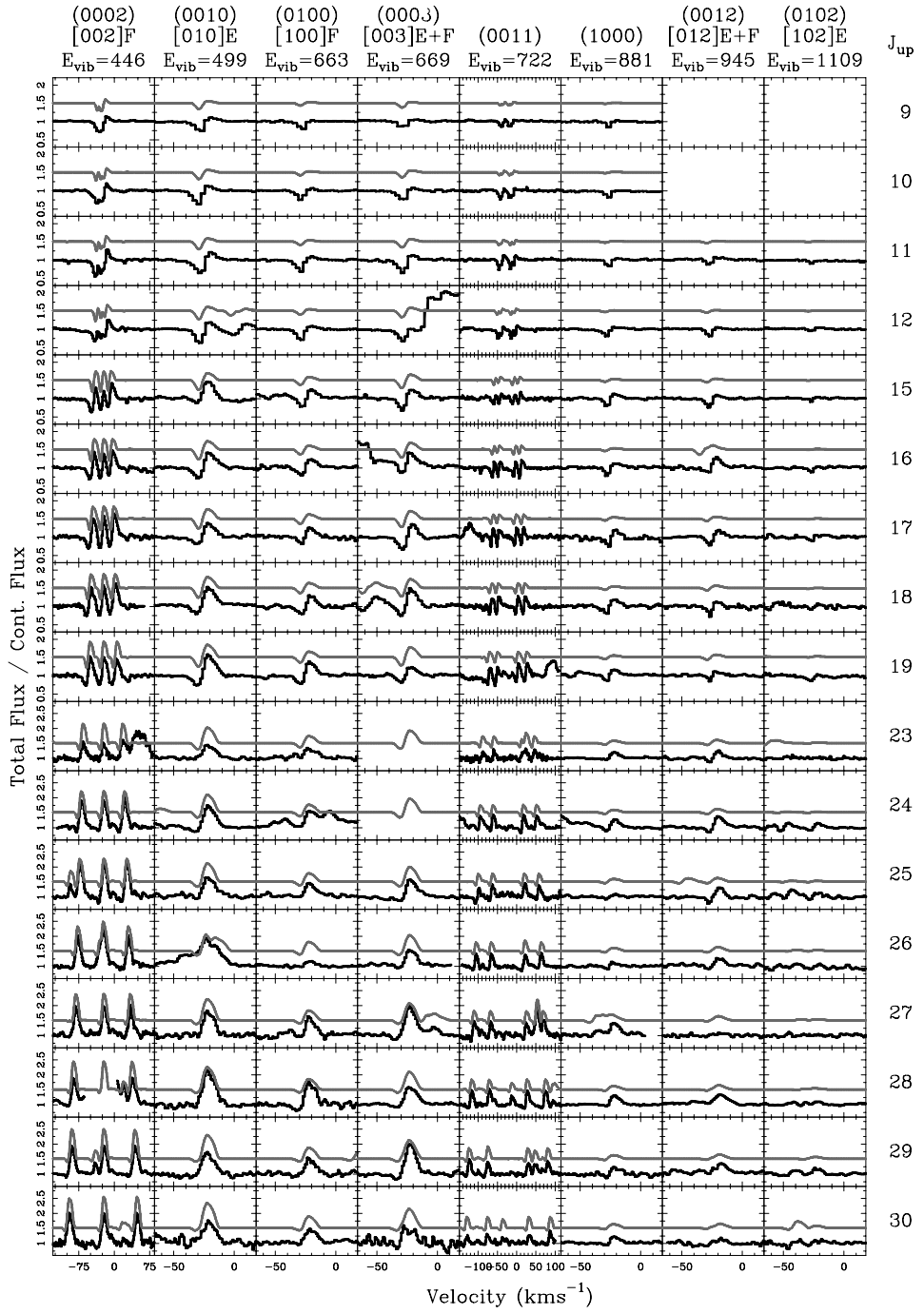

FIG. 6.—Observed HC$_3$N pure rotational lines toward the protoplanetary nebula CRL 618 in several vibrationally excited states from 446 to 1109 cm^{-1} compared with the results of our model. In a few cases the observation is not shown because the corresponding HC$_3$N line is totally masked by a stronger line from another molecule.

vibrational states or within the same vibrational state has been treated in our simulations.

The two parameters that we have tried to determine by looking at χ in a grid of models are the temperature of the gas and the HC$_3$N column density. In order to illustrate how the best solution (Fig. 6) is found, we show in Figure 7 the values of the parameter χ as a function of these two parameters. The overall set of parameters characterizing the slowly expanding molecular envelope is then shown in Table 3.

The kinetic temperature found here (250–275 K) is in very good agreement with the value derived from *Infrared Space Observatory* (*ISO*) IR data by Cernicharo et al. (2001a, 2001b). The average column density of absorbing HC$_3$N in front of

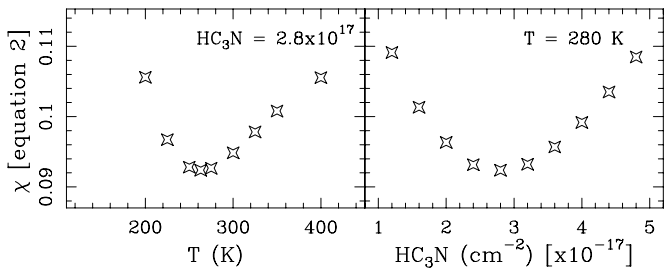

FIG. 7.—Value of χ (defined in eq. [2]) for the grid of models run to find the temperature of the CRL 618 slowly expanding envelope and the HC$_3$N column density that best fits the data shown in Fig. 6.

TABLE 3
Model Parameters of the Expanding Envelope That Provides the Best Fit to the Data Shown in Fig. 6

Parameter	Value
θ_g (arcsec)	1.5
r_d	0.7
i (deg)	90
$T_{\rm gas}$ (at $\theta = \theta_c$) (K)	263
$T_{\rm gas}$ (at $\theta = \theta_g$) (K)	263
v_r (at $\theta = \theta_c$) (km s^{-1})	5.0
v_r (at $\theta = \theta_g$) (km s^{-1})	12.0
v_{xy} (at $\theta = \theta_c$) (km s^{-1})	0.0
v_{xy} (at $\theta = \theta_g$) (km s^{-1})	6.0
$v_{\rm turb}$ (at $\theta = \theta_c$) (km s^{-1})	3.5
$v_{\rm turb}$ (at $\theta = \theta_g$) (km s^{-1})	3.5
[HC_3N] (at $\theta = \theta_c$) (cm^{-3})	154
d	-1.8
HC_3N column density (at $p < r_c$) (cm^{-2})	$(2.0–3.5) \times 10^{17}$

the continuum source is found to be in the range $(2.0–3.5) \times 10^{17}$ cm^{-2}. HC_3N column densities in front of the continuum source were determined to be 5×10^{16} cm^{-2} by Cernicharo et al. (2001b) from *ISO* observations of HC_3N (0100) and (0001) bending modes in absorption around 14 μm. The difference between both estimates could be related to two facts: First, the *ISO* data lack the spectral resolution needed to fully resolve the individual lines used for the estimate. Second, Cernicharo et al. (2001b) assumed the same filling factor for the continuum source and the absorbing gas. However, dust emission at the wavelength of the (0100) mode of HC_3N, and in particular at that of the (0001) mode, could be contributed from a region larger than the zone where HC_3N is produced. The IR *ISO* data could give the same HC_3N column density as that derived here from the millimeter lines, if the continuum level to be considered for the former calculation (originating from behind the gas) were only about 30%–50% of the total observed continuum flux at 14 μm.

6. CONCLUSIONS

In this paper we have shown the following for observations toward the protoplanetary nebula CRL 618:

1. HC_3N is detected in its ground and other vibrational states with energies up to 1100 cm^{-1}. The $J_{\rm up}$ range surveyed is from 9 to 30 (IRAM 30 m telescope, 15 vibrational states detected) and from 31 to 39 (CSO telescope, detections in five, possibly six vibrational states). The observed frequencies match very well those provided by the model of Fayt et al. (2004).

2. The line profiles of the HC_3N ground vibrational state show evidence of the HVMW already found in the strong lines of CO, HCN, and HCO^+ with the same velocity span ($\sim$200 km s^{-1}). Other vibrational states do not show this component in their rotational lines, except for the (0001) state, which shows it marginally in the lowest J-lines. Absorption features in the rotational lines of the ground vibrational state appear at velocities similar to those of features already seen in CO and HCN. The only exception is the one centered at approximately -37 km s^{-1} that is due to blending with (0100) [1 0 0]E lines.

3. The pure rotational transitions in vibrationally excited states of HC_3N show an evolution in their line profiles with increasing J, going from almost pure absorption centered at around -27 or -28 km s^{-1}, to P Cygni profiles, and finally to pure emission centered quite close to the LSR velocity of the source. The intermediate-J P Cygni profiles have the emission part also centered quite close to the LSR velocity, while the minimum of the absorption part shifts to more negative velocities and becomes less deep as J increases. The exact value of $J_{\rm up}$ at which the absorption disappears changes only slightly with the vibrational state; it happens at slightly higher values as the energy of the vibrational state increases. For example, no absorption is observed in the $J = 24–23$ transition of the (0001) vibrational state, whereas some absorption is still seen in the $J = 26–25$ line of the (1000) state. Some rotational lines within the (0001) state still trace velocities larger than those in the other vibrationally excited states.

4. A model for the slowly expanding envelope under LTE, built to explore the physical parameters that explain the extensive set of HC_3N rotational lines detected ($\sim$300, although the fit has been done to a subset of 116), has shown the following:

(*a*) The size of the inner continuum source is $\sim 0\farcs27$, with an effective temperature of $\sim$3900 K at 200 GHz and a spectral index of -1.12.

(*b*) The external size of this slowly expanding envelope is $\sim\theta = 1\farcs5$.

(*c*) The expansion velocity field has a radial component ranging from 5 to 12 km s^{-1}, with a possible extra azimuthal component reaching 6 km s^{-1} at $\theta = 1\farcs5$.

(*d*) The turbulence velocity is $\sim$3.5 km s^{-1}.

(*e*) The temperature of the envelope is in the range 250–275 K.

(*f*) The HC_3N column density in front of the continuum source is in the range $(2.0–3.5) \times 10^{17}$ cm^{-2} (the best fit is obtained for 2.8×10^{17} cm^{-2}).

The authors are grateful to the IRAM 30 m staff for providing assistance during the observations. This work has been supported by NSF grant ATM 96-16766 and by Spanish DGES and PNIE grants ESP 2002-01627, AYA 2002-10113-E, and AYA 2003-02785-E. CSO operations were supported by NSF grant AST 99-80846.

REFERENCES

Bell, M. B., Feldman, P. A., Travers, M. J., McCarthy, M. C., Gottlieb, C. A., & Thaddeus, P. 1997, ApJ, 483, L61
Bujarrabal, V., Gómez-González, J., Bachiller, R., & Martín-Pintado, J. 1988, A&A, 204, 242
Cernicharo, J. 2004, ApJ, 608, L41
Cernicharo, J., Guélin, M., Martín-Pintado, J., Peñalver, J., & Mauersberger, M. 1989, A&A, 222, L1
Cernicharo, J., Guélin, M., Menten, K. M., & Walmsley, C. M. 1987, A&A, 181, L1
Cernicharo, J., Heras, A. M., Pardo, J. R., Tielens, A. G. G. M., Guélin, M., Dartois, E., Neri, R., & Waters, L. B. F. M. 2001a, ApJ, 546, L127
Cernicharo, J., Heras, A. M., Tielens, A. G. G. M., Pardo, J. R., Herpin, F., Guélin, M., & Waters, L. B. F. M. 2001b, ApJ, 546, L123
Cox, P., Huggins, P. J., Maillard, J.-P., Muthu, C., Bachiller, R., & Forveille, T. 2003, ApJ, 586, L87
Fayt, A., et al. 2004, J. Mol. Struct., in press
Guélin, M., & Cernicharo, J. 1991, A&A, 244, L21
Herpin, F., Goicoechea, J. R., Pardo, J. R., & Cernicharo, J. 2002, ApJ, 577, 961
Kwok, S., & Bignell, R. C. 1984, ApJ, 276, 544
Kwok, S., & Feldman, P. A. 1981, ApJ, 247, L67
Martín-Pintado, J., Bujarrabal, V., Bachiller, R., Gómez-González, J., & Planesas, P. 1988, A&A, 197, L15

Martín-Pintado, J., Gaume, R., Bachiller, R., & Johnston, K. 1993, ApJ, 419, 725
Martín-Pintado, J., Gaume, R. A., Johnston, K. J., & Bachiller, R. 1995, ApJ, 446, 687
Mbosei, L., Fayt, A., Dréan, P., & Cosléou, J. 2000, J. Mol. Structure, 517, 271
Neri, R., Garcia-Burillo, S., Guélin, M., Cernicharo, J., Guilloteau, S., & Lucas, R. 1992, A&A, 262, 544
Sánchez-Contreras, C., & Sahai, R. 2004, ApJ, 602, 960
Shibata, K. M., Deguchi, S., Hirano, N., Kameya, O., & Tamura, S. 1993, ApJ, 415, 708
Spergel, D. N., Giuliani, J. L., Jr., & Knapp, G. R. 1983, ApJ, 275, 330
Thorwirth, S., Wyrowski, F., Schilke, P., Menten, K. M., Brünken, S., Müller, H. S. P., & Winnewisser, G. 2003, ApJ, 586, 338
Walmsley, M., Chini, R., Kreysa, E., Steppe, H., & Omont, A. 1991, A&A, 248, 555
Wyrowski, F., Schilke, P., Thorwirth, S., Menten, K. M., & Winnewisser, G. 2003, ApJ, 586, 344
Wyrowski, F., Schilke, P., & Walmsley, C. M. 1999, A&A, 341, 882